Efficiency comparison of spatial and spectral diversity techniques for fading mitigation in free-space optical communications over tactical-range distances

Jean Minet[a], Mikhail A. Vorontsov[a,b], G. Wu[b] and Daniel Dolfi[c]

[a]Intelligent Optics Laboratory, School of Engineering, University of Dayton, 300 College Park, Dayton, Ohio 45469-2951, USA;
[b]Optonicus, 711 E. Monument Avenue, Suite 101, Dayton, Ohio 45402, USA;
[c]Thales Research and Technology – France, RD128, 91767 Palaiseau Cedex, France

ABSTRACT

In long-range situations, the performance of free-space optical (FSO) communication links is strongly impacted by atmospheric turbulence. In this paper we compare efficiency of turbulence effects mitigation in FSO communication links using spectral (wavelength) and spatial diversity techniques. Numerical analysis of both techniques is performed considering FSO communication setting with single-mode fiber-collimator transceivers. In the case of spectral diversity setting, the fiber-collimators are based on the use of photonic crystal fibers that provide single-mode operation for three distinct wavelengths (532, 1064 and 1550nm). In the spatial diversity communication setting, analysis is performed using multiple-transceiver configurations. Analysis includes both received signal's statistical and temporal spectral characteristics.

Keywords: Free-space optical communication, atmospheric turbulence, spectral diversity, spatial diversity

1. INTRODUCTION

In long-range situations, the performance of free-space optical (FSO) communication links is strongly impacted by atmospheric turbulence. This turbulence can cause the received signal to be faded by several orders or magnitude during several milliseconds. It is thus essential to use fading mitigation techniques to improve the reliability of communication. Various techniques such as adaptive optics,[1] error coding and interleaving,[2] or maximum likelihood sequence detection,[3] have been suggested to mitigate effect of signal fading. We focus here on diversity techniques which consist in transmitting the same data through different channels that do not experience the same fades. This diversity can be spatial,[4,5] spectral,[6] or temporal.[2] Spatial diversity requires multiple transmitters and/or multiple receivers. Spectral diversity makes use of distinct wavelengths to transmit the data. Finally, temporal diversity requires a signal to be transmitted at least twice, separated by a time delay.

In what follows, we investigate numerically spatial and spectral diversity techniques for fading mitigation in a 7 km-long FSO communication link based on the use of single-mode fiber-collimator transceivers. We first consider spatial diversity FSO communication setting in which the fiber collimators are based on the on the use of photonic crystal fibers that provide single-mode operation for three distinct wavelengths (532, 1064 and 1550nm). In a second time, we analyze the performance of different spatial diversity configurations using multiple transmitters and/or multiple receivers. Statistical analysis of the power-in-fiber signals is performed through numerical simulations of laser beam propagation. Preliminary experimental results of receiver diversity are also reported.

2. METHODOLOGY OF NUMERICAL MODELING

In this paper, we investigate the efficiency of different configurations of spatial and spectral diversity techniques in a single reference scenario. This scenario corresponds to a ground-to-ground communication link over a 7 km distance.

Further author information:
M.A.V.: E-mail: mvorontsov1@udayton.edu, Telephone: 1 937 229 2797

Free-Space Laser Communication and Atmospheric Propagation XXV, edited by Hamid Hemmati, Don M. Boroson, Proc. of SPIE Vol. 8610, 86100X · © 2013 SPIE
CCC code: 0277-786X/13/$18 · doi: 10.1117/12.2007321

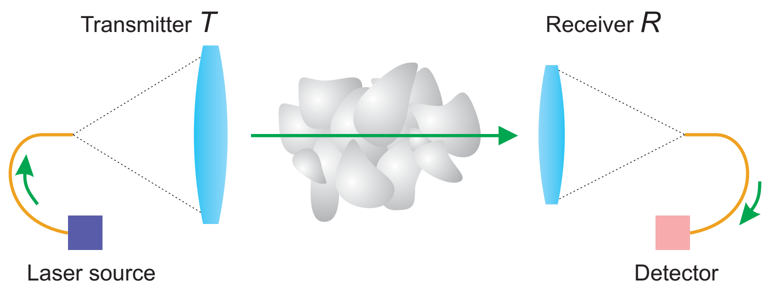

Figure 1. Schematic of a simple FSO communication link based on single-mode fiber collimator (SMFC) transmitter and receiver.

2.1 Numerical modeling of the turbulent atmosphere

The statistical properties of the atmospheric turbulence are considered to be homogeneous and isotropic over the propagation path. Under these assumptions, the spatial statistical properties of refractive-index $n(\mathbf{r})$ can be described by the spatial power spectral density $\Phi_n(\kappa)$ of refractive-index fluctuations. It is related to its covariance function $B_n(\mathbf{r})$ by the Fourier transform

$$\Phi_n(\kappa) = \frac{1}{(2\pi)^3} \iiint B_n(\mathbf{r}) \exp\left[-i\mathbf{k}\cdot\mathbf{r}\right] \mathrm{d}\mathbf{r}, \tag{1}$$

where $\kappa = |\mathbf{k}|$ is the scalar wave number.[7] For simplicity, we assume that the power spectral density for refractive-index fluctuations $\Phi_n(\kappa)$ follows the well-known Kolmogorov spectrum

$$\Phi_n(\kappa) = 0.033\, C_n^2\, \kappa^{-11/3}, \tag{2}$$

where C_n^2 is the index-of-refraction structure parameter. Typical values of this parameter range from $C_n^2 = 10^{-17}\,\mathrm{m}^{-2/3}$ (very weak turbulence) to $10^{-13}\,\mathrm{m}^{-2/3}$ (very strong turbulence). In the reference scenario considered, we use a value of $10^{-14}\,\mathrm{m}^{-2/3}$ that is typical of difficult ground-to-ground situations. Tridimensional refractive index fluctuations are represented by a set of ten equidistant and statistically independent thin random phase screens. These phase screens are statistically independent and evenly distributed along the propagation path. Temporal statistics of the atmospheric turbulence are modeled using Taylor's "frozen turbulence" hypothesis. Temporal variations of the phase screens are produced by translation of each phase screen at a constant speed of 5m/s. Each phase screen is generated using the infinitely long screen technique[8] which allows continuous simulation of the temporal evolution of turbulence over arbitrarily long periods of time.

2.2 Numerical simulation of optical-wave propagation

Figure 1 gives an example of a simple FSO communication setup based on two single-mode fiber collimator (SMFC) transceivers. A SMFC transceiver is based on a single-mode fiber whose tip is located on the focal plane of a collimating lens. The transmitted complex amplitude $A_{\mathrm{out}}(\mathbf{r})$ at the pupil plane of a transceiver is approximated by a truncated Gaussian profile:

$$A_{\mathrm{out}}(\mathbf{r}) = A_0 \exp\left(-\frac{r^2}{w_p^2}\right) \Pi_a(\mathbf{r}), \tag{3}$$

where w_p is the $1/e$ mode field radius in the pupil plane and $\Pi_a(\mathbf{r})$ is the transmitter pupil function that takes a value of one inside the circular pupil of radius pupil a and zero outside. The mode field radius w_p in the pupil plane can be expressed by the $1/e$ mode field radius w_f in the focal plane*

$$w_p = w_f \sqrt{1 + \left(\frac{\lambda f}{\pi w_f^2}\right)^2} \simeq \frac{\lambda f}{\pi w_f}. \tag{4}$$

*The $1/e$ mode field radius w_f is related to the $1/e^2$ mode field diameter MFD by the relation $MFD = \sqrt{2} w_f$.

The transmitted complex amplitude $A_{\text{out}}(r)$ is uniformly sampled on a 1024×1024 pixels grid that covers an area of $1.5 \times 1.5\,\text{m}^2$. It is then propagated using the standard split-step Fourier-transform algorithm.[9] Let $A_{\text{in}}(r)$ be the field in the receiver's pupil plane. The power P_c coupled in the receiver's fiber is obtained through the overlap integral

$$P_c = \left| \int A_{\text{in}}(r) M_{0,P}^*(\mathbf{r}) \mathrm{d}^2\mathbf{r} \right|^2, \tag{5}$$

where $M_{0,P}(\mathbf{r})$ is the receiver's mode in the pupil plane given by

$$M_{0,P}(\mathbf{r}) = M_0 \exp\left(-\frac{r^2}{w_p^2}\right) \Pi_a(\mathbf{r}), \tag{6}$$

where w_p is the receiver's mode field radius in the pupil plane, $\Pi_a(\mathbf{r})$ is the receiver's pupil function, and M_0 is a normalizing constant chosen so as $\int M_{0,P}(\mathbf{r}) M_{0,P}^*(\mathbf{r}) \mathrm{d}^2\mathbf{r} = 1$.

2.3 Simultaneous propagation of multiple wavelengths

In order to study spectral diversity settings, we need to consider simultaneous propagation of optical waves at different wavelengths λ_i, $i \in [1, N_\lambda]$. Let $\phi_\lambda(x, y)$ be the phase screen corresponding to propagation at wavelength λ through a certain slab of turbulent atmosphere. The phase screens $\phi_{\lambda_i}(x, y)$ must be obtained from a unique realization of a random process. Therefore, we first generate a phase screen $\phi_{\lambda_0}(x, y)$ for a reference wavelength $\lambda_0 = 1\,\mu$m. This phase screen is a realization of a random process with power-spectral density

$$\Phi_\phi(\kappa) = 0.207 \left(\frac{2\pi}{\lambda_0}\right)^2 C_n^2\, \Delta z\, \kappa^{-11/3}, \tag{7}$$

where Δz is the thickness of the slab corresponding to the phase screen and $C_n^2 = C_{n(\lambda_0)}^2$. If we neglect variation of air refractivity with wavelength, the phase screen at wavelength λ_i can be simply obtained by multiplying the reference phase screen by a factor λ_0/λ_i. For given pressure P and temperature T, the index of refraction of air at wavelength λ is given by the relation

$$n(\lambda) = 1 + A(\lambda)\frac{P}{T}, \tag{8}$$

where $A(\lambda)$ is the reduced refractivity of dry air. $A(\lambda)$ can be computed using the Sellmeier's equation[10,11]

$$A(\lambda) = 10^{-10}\left[8342.13 + 2406030\left(130 - \lambda_0^2/\lambda^2\right)^{-1} + 15997\left(38.9 - \lambda_0^2/\lambda^2\right)^{-1}\right]\frac{288.15}{1013.25}, \tag{9}$$

where $\lambda_0 = 1\,\mu$m. Taking into account the variation of air refractivity with wavelength, we obtain the phase screen at wavelength λ_i from the reference phase screen

$$\phi_{\lambda_i}(x, y) = \frac{\lambda_0}{\lambda_i}\frac{A(\lambda_i)}{A(\lambda_0)}\phi_{\lambda_0}(x, y). \tag{10}$$

The earth's atmosphere exhibits an index of refraction gradient caused by variation of air density with altitude. Since this gradient is wavelength dependent, beams of different wavelengths will take different paths from the transmitter to the receiver and will thus encounter different refractive index fluctuations. One can show from the ideal gas law that the pressure $P(h)$, where h is altitude, satisfies the following differential equation

$$\frac{\mathrm{d}P}{\mathrm{d}h} = -\frac{Mg(h)}{R}\frac{P(h)}{T(h)}, \tag{11}$$

where $M = 28.964 \times 10^{-3}$ kg/mol is molecular mass of dry air, $R = 8.314472\,\text{J}\,\text{K}^{-1}\,\text{mol}^{-1}$ is ideal gas constant, and $g(h)$ is the acceleration of gravity that can be considered constant for small altitudes ($g(h) = g = 9.80665\,\text{m}\,\text{s}^{-2}$).

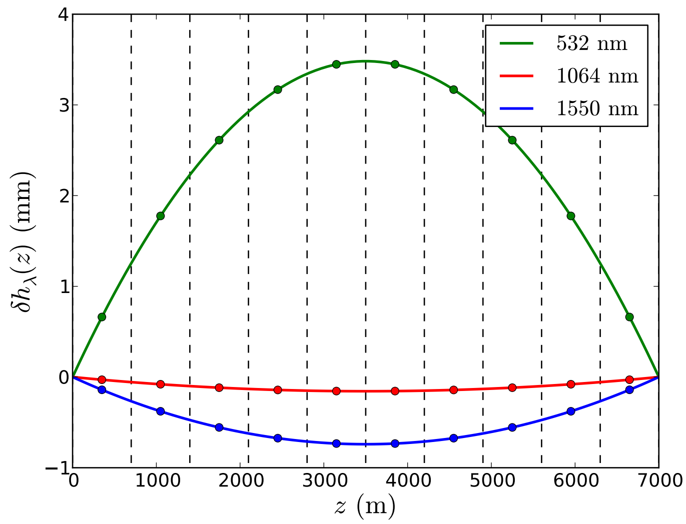

Figure 2. Vertical phase screen shifts $\delta h_{\lambda_i}(z)$). The 7 km-long propagation volume is divided in 10 slabs separated by dotted lines in the figure. The circular dots are located in the centers of each phase screen.

According to the US1976 model of standard atmosphere, air temperature in the troposphere decreases linearly with altitude: $T(h) = T_0 + \alpha h$, where $\alpha = 6.5 \times 10^{-3}$ K/m. One can thus solve Eq. 11 and use 8 to obtain

$$n(h) = 1 + A(\lambda)\frac{P_0}{T_0}\left(\frac{T_0}{T_0 + \alpha h}\right)^{\frac{Mg}{R\alpha}-1}, \tag{12}$$

where P_0 and T_0 are respectively air pressure and temperature at sea level. From the eikonal equation, one can show that the ray-position vector $\mathbf{r}$ satisfies the differential equation[12]

$$\frac{\mathrm{d}}{\mathrm{d}s}\left(n\frac{\mathrm{d}\mathbf{r}}{\mathrm{d}s}\right) = \nabla n, \tag{13}$$

where s is the scalar distance along the ray. Note that in Eq. 13, n can be considered to be constant and equal to 1. For short and nearly horizontal path of altitude h_0, earth curvature may be neglected and refractive index gradient may be considered to be constant such as Eq. 13 reduces to

$$\frac{\mathrm{d}^2 h}{\mathrm{d}z^2} = \gamma(\lambda), \tag{14}$$

where h is the height of the ray, z is the horizontal coordinate and

$$\gamma(\lambda) = \frac{\mathrm{d}n}{\mathrm{d}h}(h_0) = -A(\lambda)\left(\frac{Mg}{R} + \alpha\right) P_0 T_0^{\frac{Mg}{R\alpha}} \left(T_0 + \alpha h_0\right)^{-\frac{Mg}{R\alpha}-2}. \tag{15}$$

Therefore, a ray of wavelength λ propagating between the points $A(z = 0, h = h_0)$ and $B(z = L, h = h_0)$ follows the parabolic path $h_\lambda(z) = \frac{\gamma(\lambda)}{2} z(z-L) + h_0$. The phase screens $\phi_{\lambda_i}(x, y)$ are thus obtained by shifting vertically the scaled version of the reference phase screen.

$$\phi_{\lambda_i}(x, y) = \frac{\lambda_0}{\lambda_i}\frac{A(\lambda_i)}{A(\lambda_0)}\phi_{\lambda_0}(x, y - \delta h_{\lambda_i}(z)), \tag{16}$$

where $\delta h_{\lambda_i}(z) = \frac{1}{2}\left[\gamma(\lambda_i) - \gamma(\lambda_0)\right] z(z - L)$ and z is the longitudinal position of the corresponding phase screen.

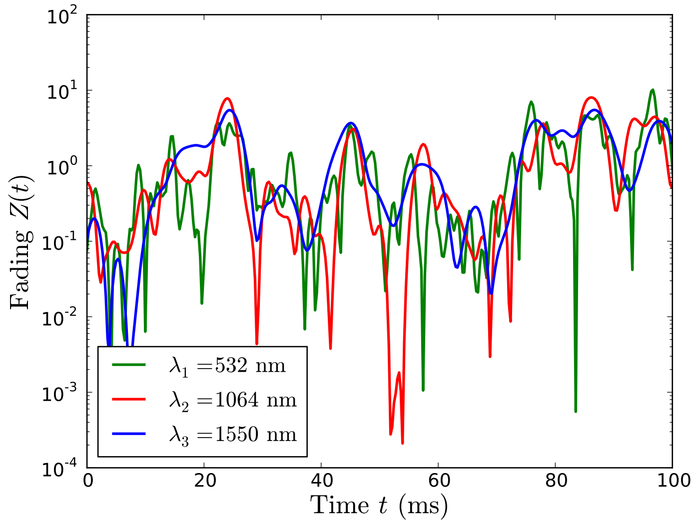

Figure 3. Temporal evolution of the turbulence-induced fadings $Z(t)$ at wavelengths $\lambda_1 = 532$ nm, $\lambda_2 = 1064$ nm and $\lambda_3 = 1550$ nm.

3. SPECTRAL DIVERSITY

In this section, we consider a laser communication setup that consists of two identical transceivers. Each transceiver is based on a photonic crystal fiber whose mode is considered Gaussian and independent on wavelength (mode field diameter $MFD = 10\,\mu$m). The fiber end is positioned on the focal plane of a collimating achromatic lens of focal length $f = 175$ mm and aperture radius $a = 16.5$ mm. Each transceiver is thus capable of transmitting or receiving simultaneously signal at three wavelengths $\lambda_1 = 532$ nm, $\lambda_2 = 1064$ nm and $\lambda_3 = 1550$ nm. Let $P_i(t)$ be the instantaneous power received in the fiber at wavelength λ_i and time t. $P_i(t)$ can be expressed in the form

$$P_i(t) = Z_i(t)\langle P_i \rangle, \tag{17}$$

where $\langle P_i \rangle$ is the average of $P_i(t)$ and $Z_i(t)$ is a dimensionless variable describing tuburlence-induced fading of the received signal at wavelength λ_i. We performed numerical simulations of optical wave propagation using the method and parameters described in Section 2. As a result, we obtained three sequences $Z_i(t_j)$, $i \in \{1, 2, 3\}$, where $\{t_j, i = 1, \ldots, 4 \times 10^{-5}\}$ is a sequence of equidistant times of duration 78.125 s. The first 100 ms of the temporal evolution of turbulence-induced fadings $Z_i(t)$ are represented in Fig. 3. Table 1 gives estimates of the covariance and correlation matrices of the random vector $\ln \mathbf{Z} = [\ln Z_1, \ln Z_2, \ln Z_3]^T$. As expected, correlation between turbulence-induced fadings decreases with wavelength separation. One can also observe that scintillation decreases with increasing wavelength. Figure 4 gives estimates of the cumulative distribution

Table 1. Covariance and correlation matrices of the random vector $\ln \mathbf{Z} = [\ln Z_1, \ln Z_2, \ln Z_3]^T$.

	$\ln Z_1$	$\ln Z_2$	$\ln Z_3$
$\ln Z_1$	2.513 / 1	1.006 / 0.423	0.816 / 0.398
$\ln Z_2$		2.249 / 1	1.117 / 0.576
$\ln Z_3$			1.672 / 1

function of turbulence-induced fading at each of the three considered wavelengths. The probability that $Z(t)$ is less than 10^{-2} is equal to 0.028 for $\lambda = 532$ nm, 0.023 for $\lambda = 1064$ nm, and 0.012 for $\lambda = 1550$ nm. Equal gain combining of the three received signals leads to the turbulence-induced fading $Z_m(t) = \frac{1}{3}\left[Z_1(t) + Z_2(t) + Z_3(t)\right]$.

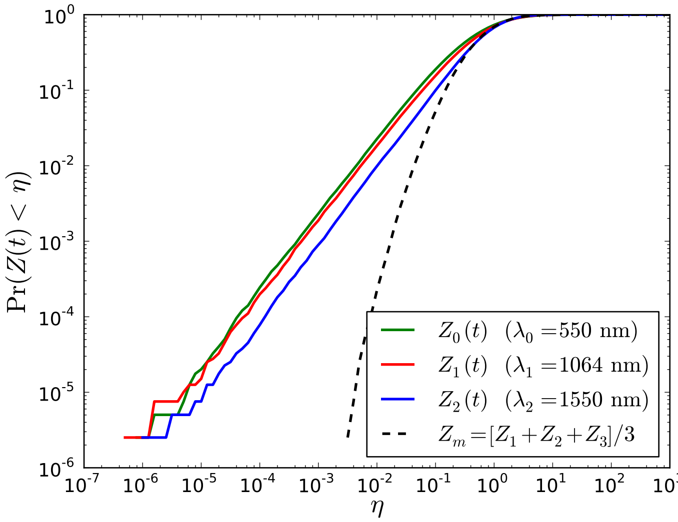

Figure 4. Estimation of the cumulative distribution function of the turulence-induced fadings $Z(t)$ at wavelengths $\lambda_1 = 532$ nm, $\lambda_2 = 1064$ nm and $\lambda_3 = 1550$ nm. The dashed curve corresponds to the fading obtained when averaging signals at the three wavelengths (equal gain combining).

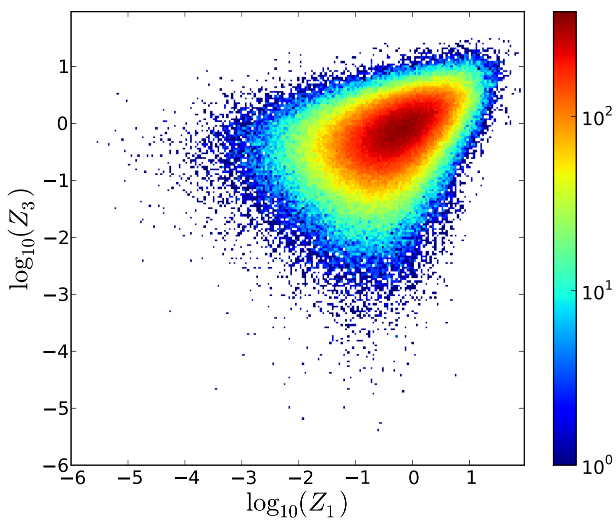

Figure 5. Two-dimensional histogram of turbulence-induced fading at wavelengths $\lambda_1 = 532$ nm and $\lambda_3 = 1550$ nm.

The cumulative distribution function of $Z_m(t)$ is represented in dashed lines in Fig. 4. The probability that $Z_m(t)$ is less than 10^{-2} is equal to 4.3×10^{-4}, which is 30 to 65 times less than the single wavelength case. Figure 5 represents the two-dimensional histogram of turbulence-induced fading at wavelengths $\lambda_1 = 532$ nm and $\lambda_3 = 1550$ nm. The joint distribution of turbulence-induced fadings differs considerably from a multivariate log-normal distribution which would have elliptical contours in Fig. 5. One can observe on this figure that large signal values are strongly correlated while small signal values are only weakly correlated. Strong fadings of the received signals are thus unlikely to occur at each of the three wavelengths simultaneously. This explains the strong spectral diversity gain observed in Fig. 4.

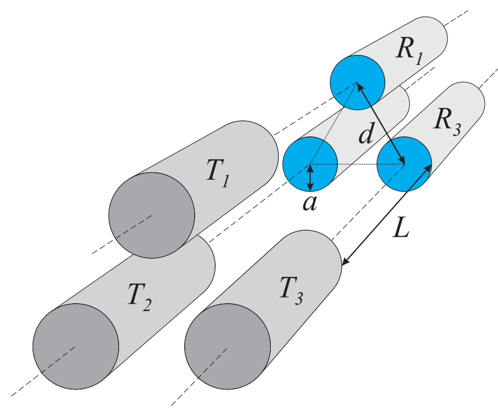

Figure 6. Geometry of the multiple transceivers configuration

4. SPATIAL DIVERSITY

4.1 Simulation results

We now consider a spatial diversity laser communication setup that consists of three transmitters and three receivers. The optical axes of the three transmitters / receivers are positioned at the vertices of an equilateral triangle of side $d = 37$ mm as shown in Figure 6. Each transceiver is virtually identical to the transceivers considered in Section 3 ($MFD = 10\,\mu$m, $f = 175$ mm, $a = 16.5$ mm.) In practice, the photonic crystal fiber used in the spectral diversity setup can be replaced by a simple single-mode fiber. The three transceivers T_i, $i \in \{1, 2, 3\}$, operate at three contiguous wavelengths within the L-band of the 100 GHz ITU grid specification ($\lambda_1 = 1549.32$ nm, $\lambda_2 = 1550.12$ nm and $\lambda_3 = 1550.92$ nm). Thanks to add/drop multiplexers, each receiver R_j, $j \in \{1, 2, 3\}$ is able to measure independently the power-signals $P_{ij}(t)$ received at the three wavelengths λ_i, $i \in \{1, 2, 3\}$. $P_{ij}(t)$ can the expressed in the form

$$P_{ij}(t) = Z_{ij}(t)\langle P_{ii}\rangle \tag{18}$$

where $\langle P_{ii}\rangle$ is the average of $P_{ii}(t)$ and $Z_{ij}(t)$ is a dimensionless variable describing turbulence-induced fading of the channel T_i to R_j. Note that because the transceiver T_i is aligned on the receiver R_i, $\langle Z_{ii}\rangle = 1$ and $\langle Z_{ij}\rangle < 1$ for $i \neq j$. Let $Z_{FD}(t) = \frac{1}{9}\sum_{i,j} Z_{ij}(t)$ be the dimensionless variable describing the turbulence-induced fading of the signal obtained by summing the nine signal P_{ij}. The cumulative distribution function of $Z_{FD}(t)$ is represented in Figure 7. On this Figure, the variable $Z_{TD}(t) = \frac{1}{3}\sum_i Z_{i1}(t)$ corresponds to a situation of transmitter diversity (3 receivers and 1 receivers) and the variable $Z_{RD}(t) = \frac{1}{3}\sum_j Z_{1j}(t)$ corresponds to a situation of receiver diversity (1 receivers and 3 transmitters). Comparison between Fig. 7 and Fig. 4 shows that transceiver-only and receiver-only spatial diversity scenarios have fading mitigation efficiencies comparable to the spectral diversity scenario described in Section 3. Because it uses 9 differents channels, the full (transmitter and receiver) diversity scenario performs better than the transmitter-only and receiver-only diversity scenarios. Figure 8 represents the two-dimensional histogram of variables $Z_{11}(t)$ and $Z_{12}(t)$. As in the spectral diversity scenario, we observe that the joint distribution of turbulence-induced fadings differs considerably from the log-normal distribution. Strong fading of the received signals are unlikely to occur at different channels simultaneously, which explain the strong spatial diversity gain observed in Fig. 7.

4.2 Preliminary experimental results

In this section, we describe preliminary experimental results of receiver diversity over a 7 km-long horizontal atmospheric link. The transmitter, placed on the rooftop of a 40m-high building, was operating at a wavelength $\lambda = 1064$ nm. It was based on a single-mode fiber collimator of aperture radius $a = 13$ mm and $1/e$ mode field radius $w_p = 11.6$ mm. The receiver diversity setup was placed 7 km-away on the fifth floor of the University of Dayton's College Park Center building at a height of 15 m. It was based on three receivers (R_j, $j \in \{1, 2, 3\}$) positioned at the vertices of an equilateral triangle of side $d = 64.1$ mm as shown in Fig. 9.[13] Each receiver

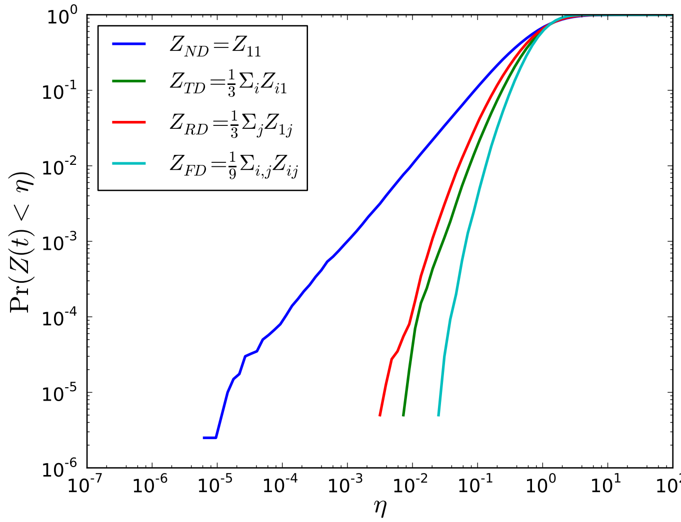

Figure 7. Estimation of the cumulative distribution function of the turulence-induced fadings $Z(t)$ in four different situations of spatial diversity: ND: no diversity, TD: transmitter diversity, RD: receiver diversity, and FD: full (transmitter and receiver) diversity.

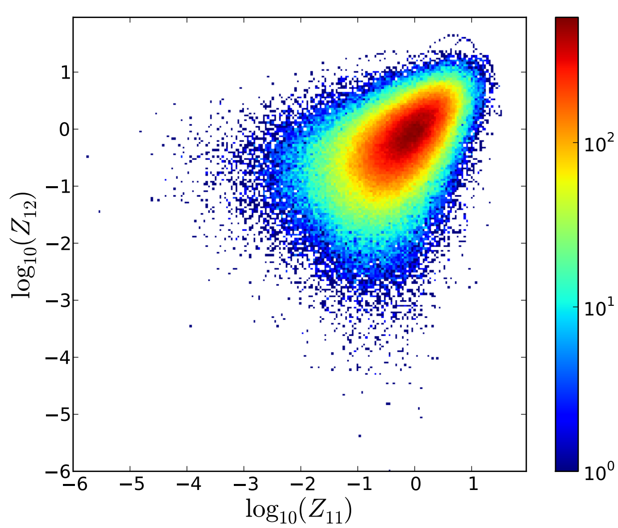

Figure 8. Two-dimensional histogram of turbulence-induced fadings $Z_{11}(t)$ and $Z_{12}(t)$.

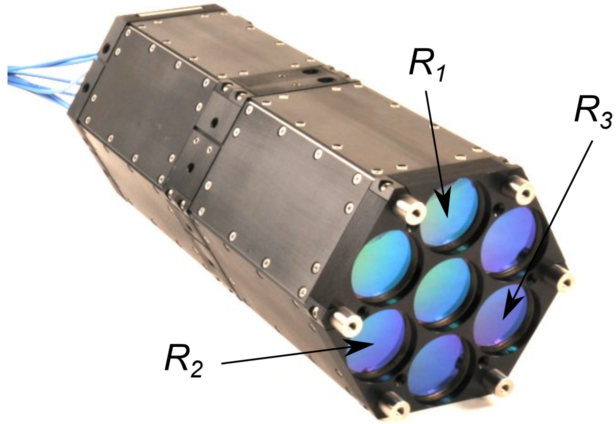

Figure 9. Optonicus' INFA receiver cluster used in the receiver diversity experiment.

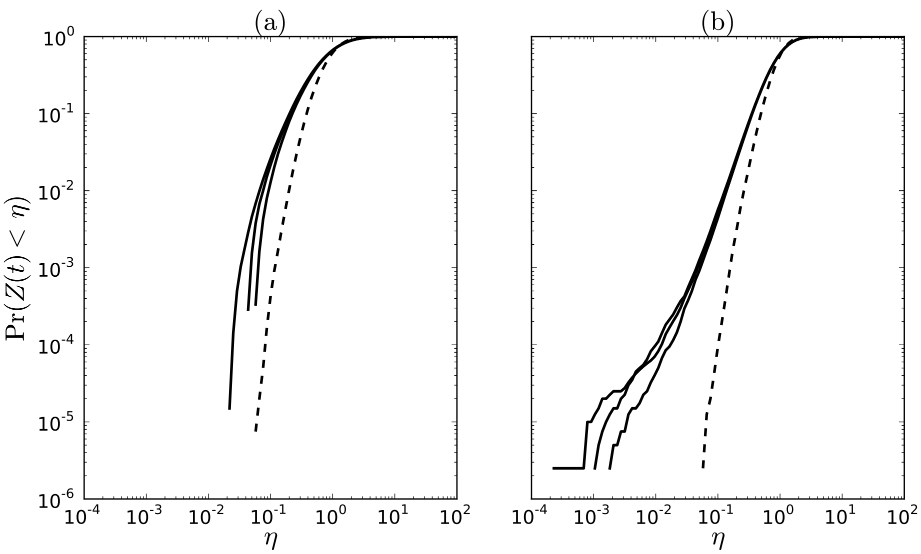

Figure 10. Estimation of the cumulative distribution function of the turbulence-induced fadings $Z(t)$ in the receiver diversity setup ((a): experiment, (b): simulation). Solid lines: $Z_j(t)$, $j \in \{1,2,3\}$, dotted line: $Z_{RD}(t) = \frac{1}{3}\sum_j Z_j(t)$.

consisted of a collimating lens of aperture radius $a = 16.5$ mm and focal length $f = 175$ mm and a single-mode fiber with mode-field diameter $MFD = 7.2\,\mu$m whose tip was positioned at the collimating lens focal point. A scintillometer (*Scintec BLS 2000*) was used to measure the refractive index structure constant $C_n^2 = 2 \times 10^{-15}\,\mathrm{m}^{-2/3}$. The three received signals $Z_j(t)$, $j \in \{1,2,3\}$ were synchronously recorded using InGaAs detectors at a sampling rate of 2 kHz during 200 s. Fig. 10(a) gives estimates of the cumulative distribution function of turbulence-induced fadings $Z_j(t)$, $j \in \{1,2,3\}$. Let $Z_{RD}(t) = \frac{1}{3}\sum_j Z_j(t)$ be the dimensionless variable describing the turbulence-induced fading of the signal obtained by equal gain combining of the three received signals. The dotted line in Fig. 10(a) represents an estimate of the cumulative distribution function of $Z_{RD}(t)$.

We performed numerical simulations of optical wave propagation using the parameters of the experiment described above. Estimates of the corresponding cumulative distribution functions are represented in Fig. 10(b). Numerical simulation results are in good agreement with the experimental results of Fig. 10(a). The difference observed for strong fadings can be explained by the limited dynamic range of the detectors used in the experiment.

Work is ongoing to improve the quality of recorded data.

5. CONCLUSION

In this paper, we performed numerical simulation of optical wave propagation to study the efficency of spatial and spectral diversity techniques for turbulence-induced fading mitigation in FSO communications. In both cases, we considered diversity setup made of three parallel channels and observed that equal-gain combining of these three channels leads to a reduction of strong fadings of more than two orders of magnitude. Both spectral and spatial diversity techniques have thus the potential of dramatically improve the performance of FSO communication systems. However, the choice between spatial and spectral diversity techniques may lead to very different systems. Spatial diversity systems may have the advantage of reduced production cost thanks to identical sub-systems while spectral diversity may lead to more compact and versatile designs at the cost of increased complexity. Note that other factors such as atmospheric absorption or detector noise must be taken into account in the final decision.

ACKNOWLEDGMENTS

The authors thank Ernst Polnau for helpul discussions. This work was supported in part by the US Air Force Office of Scientific Research MURI Contract No. FA9550-12-1-0449 and by Cooperative Agreement between the University of Dayton and Thales Research and Technology Corporation (France).

REFERENCES

[1] Weyrauch, T. and Vorontsov, M. A., "Free-space laser communications with adaptive optics: Atmospheric compensation experiments," *Journal of Optical and Fiber Communications Reports* **1**(4), 355–379 (2004).

[2] Greco, J. A., "Design of the high-speed framing, FEC, and interleaving hardware used in a 5.4km free-space optical communication experiment," *Proceedings of SPIE* **7464**, 746409–746409–7 (2009).

[3] Kahn, J., "Free-space optical communication through atmospheric turbulence channels," *IEEE Transactions on Communications* **50**(8), 1293–1300 (2002).

[4] Navidpour, S., Uysal, M., and Kavehrad, M., "BER Performance of Free-Space Optical Transmission with Spatial Diversity," *IEEE Transactions on Wireless Communications* **6**(8), 2813–2819 (2007).

[5] Walther, F. G., Moores, J. D., Murphy, R. J., Michael, S., and Nowak, G. A., "A process for free-space laser communications system design," *Proceedings of SPIE* **7464**, 74640V–74640V–9 (2009).

[6] Giggenbach, D., Wilkerson, B. L., Henniger, H., and Perlot, N., "Wavelength-diversity transmission for fading mitigation in the atmospheric optical communications channel," *Proceedings of SPIE* **6304**, 63041H–63041H–12 (2006).

[7] Andrews, L. C. and Phillips, R. L., [*Laser beam propagation through random media*], SPIE Press (1998).

[8] Vorontsov, A. M., Paramonov, P. V., Valley, M. T., and Vorontsov, M. A., "Generation of infinitely long phase screens for modeling of optical wave propagation in atmospheric turbulence," *Waves in Random and Complex Media* **18**(1) (2008).

[9] Fleck, J. A., Morris, J. R., and Feit, M. D., "Time-dependent propagation of high energy laser beams through the atmosphere," *Applied Physics* **10**(2), 129–160 (1976).

[10] Edlen, B., "The Refractive Index of Air," *Edlen, B* **71**, 70–80 (1966).

[11] van der Werf, S. Y., "Ray tracing and refraction in the modified US1976 atmosphere.," *Applied optics* **42**, 354–66 (Jan. 2003).

[12] Southwell, W. H., "Ray tracing in gradient-index media," *J. Opt. Soc. Am.* **72**(7), 908–911 (1982).

[13] www.optonicus.com.